AD-A149 533 VELOCITY MEASUREMENTS IN A 3D SHOCK WAVE LAMINAR BOUNDARY LAYER INTERACTI..(U) VON KARMAN INST FOR FLUID DYNAMICS RHODE-SAINT-GENESE (BELGIU.. G DEGREZ ET AL. 1/1

UNCLASSIFIED 30 SEP 84 VKI-CR-84-29 AFOSR-TR-84-1225 F/G 20/4 NL

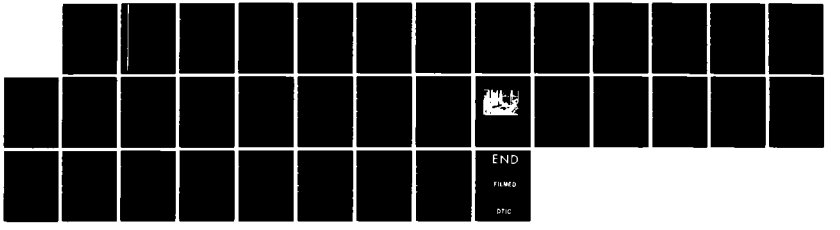

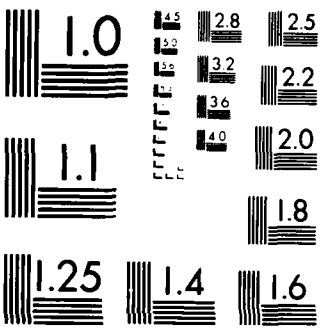

AFOSR-TR- 84-1225

GRANT AFOSR 83-0273

VELOCITY MEASUREMENTS IN A 3D SHOCK WAVE LAMINAR BOUNDARY LAYER INTERACTION
PART 1 - LOW SPEED 2D LDV MEASUREMENTS

G. DEGREZ AND J.J. GINOUX

VON KARMAN INSTITUTE FOR FLUID DYNAMICS
CHAUSSÉE DE WATERLOO, 72
B - 1640 RHODE SAINT GENÈSE - BELGIUM

SEPTEMBER 30, 1984

INTERIM SCIENTIFIC REPORT
01 AUGUST 1983 - 31 JULY 1984

PREPARED FOR

AFOSR/PKN BOLLING AFB DC 20332
AND
EUROPEAN OFFICE OF AEROSPACE RESEARCH AND DEVELOPMENT
LONDON, UK

TABLE OF CONTENTS

UNCLASSIFIED
SECURITY CLASSIFICATION OF THIS PAGE (When Data Entered)

REPORT DOCUMENTATION PAGE

READ INSTRUCTIONS BEFORE COMPLETING FORM

1. REPORT NUMBER: AFOSR-TR- 25
2. GOVT ACCESSION NO.: AD A147533
3. RECIPIENT'S CATALOG NUMBER:

4. TITLE (and Subtitle)
VELOCITY MEASUREMENTS IN A 3D SHOCK WAVE LAMINAR BOUNDARY LAYER INTERACTION
Part 1 - Low speed 2D LDV measurements

5. TYPE OF REPORT & PERIOD COVERED
Interim Scientific Report
01 Aug.83 - 31 Jul 84

6. PERFORMING ORG. REPORT NUMBER
VKI CR 84-29

7. AUTHOR(s)
G. Degrez & J.J. Ginoux

8. CONTRACT OR GRANT NUMBER(s)
Grant AFOSR 83-0273

9. PERFORMING ORGANIZATION NAME AND ADDRESS
von Karman Institute for Fluid Dynamics
Chaussée de Waterloo, 72
B - 1640 Rhode Saint Genèse - Belgium

10. PROGRAM ELEMENT, PROJECT, TASK AREA & WORK UNIT NUMBERS
61102F
2307/A1

11. CONTROLLING OFFICE NAME AND ADDRESS
AIR FORCE OFFICE OF SCIENTIFIC RESCH/NA
BOLLING AFB, DC 20332

12. REPORT DATE
30 Sept 84

13. NUMBER OF PAGES
31

14. MONITORING AGENCY NAME & ADDRESS(if different from Controlling Office)

15. SECURITY CLASS. (of this report)
UNCLASSIFIED

15a. DECLASSIFICATION DOWNGRADING SCHEDULE

16. DISTRIBUTION STATEMENT (of this Report)
Approved for public release;
Distribution unlimited.

17. DISTRIBUTION STATEMENT (of the abstract entered in Block 20, if different from Report)

18. SUPPLEMENTARY NOTES

19. KEY WORDS (Continue on reverse side if necessary and identify by block number)
Two dimensional incompressible viscous flow
Laminar boundary layer/separation
(Laser doppler velocimetry)

20. ABSTRACT (Continue on reverse side if necessary and identify by block number)

Single component LDV measurements were obtained in the separated 2D thin laminar boundary layer over an elliptic cylinder. The ellipse had an axis ratio of 4:1 and the incoming Reynolds numbers based on the minor axis were 675 and 1350. Velocity measurements were obtained within 0.05 mm from the surface both in attached and reverse flow regions. Painting the model with matt black paint and covering the tunnel walls proved to be effective means of improving signal quality. Measurements were successful both in back and forward scatter modes. The velocity profiles measured with Bragg cells indicate that the flow is separated at the ellipse mid-chord and that the separation bubble extends far downstream in the wake. The velocity profiles in the attached flow region compare well with the results of a boundary layer computation.

DD FORM 1 JAN 73 1473 EDITION OF 1 NOV 65 IS OBSOLETE

UNCLASSIFIED

SECURITY CLASSIFICATION OF THIS PAGE (When Data Entered)

ACKNOWLEDGEMENTS

The cooperation of Professor J.F. Wendt in defining and organizing the test program, of S. Olçmen for the measurements of sections 3.1 to 3.4, and of R. Arina for the boundary layer computation is gratefully acknowledged.

LIST OF SYMBOLS

s,n	coordinate system along ellipse surface
	s : distance along the surface from the leading edge
	n : coordinate normal to the surface
x,y,z	Cartesian coordinate system
	x : along ellipse major axis
	y : along the cylinder generatrix
	z : along ellipse minor axis
L'	ellipse half perimeter
V	velocity
V_∞	freestream velocity

LIST OF FIGURES

1. INTRODUCTION

The rapid development of computational methods for solving the Navier-Stokes equations has stimulated a renewed interest in laminar separated flows at high Reynolds numbers. Indeed, for the purpose of evaluating the qualities of various computational schemes, laminar test cases are preferable to turbulent cases because of the uncertainty associated with turbulence modelling. Unfortunately, laminar separated flows at high Reynolds numbers are often unstable and only very few data sets are available (Refs. 1-2). Three dimensional data are particularly lacking.

With the sponsorship of AFOSR, the von Karman Institute has undertaken a program of studies to provide a complete data set on a three dimensional shock wave laminar boundary layer interaction. First, surface flow data have been collected and analyzed under Grant AFOSR 82-0051 (Refs. 3-4). This research showed the existence of a large region of separated flow and proved that the three dimensional skewed shock laminar boundary layer interaction could be correlated by a functional form similar to turbulent correlations.

Surface flow data provide only partial information on the flowfield. In addition, velocity distributions are required. Obtaining these velocity distributions represents a major experimental challenge because of the combination of high speed, three dimensionality, the need for high spatial resolution and the proximity of solid surfaces. To overcome these difficulties, Laser Doppler Velocimetry appears to be the best suited technique. With this technique, fluid velocities are measured by observing the doppler shift in the frequency of laser light scattered by small particles moving with the fluid. The main advantage of LDV is that no probe needs to be inserted in the flow and that it does not require calibration. Furthermore, flow compressibility does not represent a special complication. On the other hand, the measured velocity is that of the scattering particles, not the fluid itself. For the measurements to be representative of the fluid velocity field, it must be ensured that the slip velocity of the particles is zero or at least small with respect to the measured velocity even in strong acceleration regions.

A step by step approach to the high speed three dimensional problem was outlined in the original proposal. In the first step, velocity measurements were performed in the low speed flow over an elliptic cylinder. The flow conditions provided thin laminar boundary layers separating to form a laminar bubble downstream of the cylinder. The problems addressed by this step were the need of high spatial resolution and the proximity of solid surfaces. A second step is given by the study of the two dimensional incident shock wave laminar boundary layer interaction, which adds the complication of high speed to the previous step. Despite it now being a classical flow, very few velocity data exist because of the limitations of the classical measurement techniques. The third step adds the third dimension to the problem. The approach is schematically represented in figure 1. We shall deal with the first step in this report.

In addition to the experimental results, some boundary layer computations were performed for purposes of comparison. In section 2, the experimental program is described. In section 3, we present the results of the flowfield measurements and in section 4, the data are compared with the results of the computations. Finally, section 5 presents the conclusions of this report.

2. EXPERIMENTAL PROGRAM

2.1 Facility and test configuration

The experiments were carried out in a small blowdown wind tunnel having a contraction ratio of 4:1 to ensure uniformity of the flow. To account for the boundary layer growth along the tunnel walls, a slightly diverging test section was built, designed to operate in the range 0.5 to 2.5 ms^{-1}. The streamwise uniformity of the flow was verified a posteriori. The effective test section was 12 cm × 12 cm. The facility, together with the experimental setup is shown in figure 2.

The model consisted of an elliptic cylinder having a major axis of 4 cm and a minor axis of 1 cm (4:1) which spanned the test section. It was verified that these dimensions provided an acceptable blockage effect. Blockage effects can be expressed as an increment in incoming stream velocity ΔV_∞. This can be split up in two parts, one due to solid blockage effects, the second to wake blockage effects.

$$\Delta V_\infty = V_\infty(\varepsilon_S+\varepsilon_W)$$

The expressions for ε_S and ε_W are given in reference 5. For the present model, $\varepsilon_S+\varepsilon_W = 0.0249$, i.e., 2.5% which was considered acceptable.

Two flow conditions were studied : V_∞ = 1 ms^{-1} and 2 ms^{-1}, yielding Reynolds numbers based on the minor axis of 675 and 1350, respectively. This ensured that the flow remained laminar over the entire length of the ellipse and in the separation bubble. A rough estimate of the boundary layer thickness on the body, performed using the Blasius flat plate formula, yielded a value of 2.7 mm at the trailing edge for the highest Reynolds number. This is comparable to the boundary layer thickness in the future high speed experiments.

2.2 Laser doppler velocimeter installation

2.2.1 General description

The laser velocimeter used for all LDV flow field measurements was a single velocity component, dual beam, fringe mode system with forward and backward scatter light collection. An advantage that the dual mode has over other LDV modes is that the doppler frequency measured is independent of the scattering direction. This advantage allows for relatively easy system alignment. The rate at which a fluid particle crosses the interference fringes setup by the intersecting laser beams is linearly proportional to the velocity. Forward and backward scatter were used to evaluate the possibility of both methods to achieve high resolution : the advantage of forward scatter is that it produces higher signal-to-noise ratios whereas a backscatter setup would be much easier for the three dimensional configuration (Fig. 1.3). For a detailed discussion on the principles of LDV, the reader should consult Durst et al. (Ref. 6). A schematic of the system used is shown in figure 3.

2.2.2 Transmitting optics

Two different light sources were used : in the first four series of experiments (sections 3.1 to 3.4) a 15 mW helium/neon laser produced a 1.1 mm beam of 0.6329 μm (red) wavelength. In the fifth series, a 4 W argon ion laser produced a 1.5 mm beam at a 0.5145 μm (green) wavelength. In this instance, the effective power used was adjusted between 0.1 and 0.6 watt and measured by a Spectra-Physics power meter. The beam was divided with a beam splitter into two beams and their intensity was equalized by a Spectra-Physics polarizer. In section 3.5, an OEI Bragg cell unit was used to resolve directional ambiguity. A beam spacer followed by a 2.21 beam expander provided the appropriate beam separation and beam diameter. All other things being equal, increased beam diameters produce smaller probe volumes; consequently, spatial resolution improves and signal intensity increases significantly. A converging lens was used to cross the beams, which established the measuring or "probe" volume containing the interference fringes. A summary of the basic LDV equations and system parameters, including probe volume dimensions is given in Table 1. The values presented in this table are considered nominally correct (to about 5 %).

2.2.3 Receiving optics

The light scattered by particles crossing the fringes in the probe volume was collected by a Temron zoom length. The beam intersection was focussed onto a pinhole located between the zoom lens and the RCA (type 4526) photomultiplier. The pinhole dimension was 50 μm for the first four series of experiments (sections 3.1 to 3.4) and 35 μm for the last one (section 3.5).

The optics were oriented on axis and looked down upon the beam intersection at approximately 10°-15° incidence with respect to the plane of the flat plate. The plane of the incoming beams was put at 0.5° incidence to the plate so that the bottom of the beams would run parallel to the model transverse axis.

The major difficulty in obtaining measurements close to the model surface was due to reflections. To minimize these, various configurations were examined in which the model was painted in matt black and the tunnel walls were covered. This is discussed in section 3.3.

The receiving and transmitting optical assemblies were placed on platforms on either side of the test section, which were part of a three-axes traversing table that surrounded the tunnel in the shape of a horseshoe. Movement was controlled by a Gelmo microprocessor that provided discrete positioning to 0.1 mm in the automatic mode and continuous positioning in a manual mode.

2.2.4 Processing electronics

The output signal from the photomultiplier was filtered by a series of bandpass filters, VKI instruments type DO-781-3. This produced a relatively noise-free signal which could then be processed by an electronic counter, VKI instruments type DO-78-3A. The output signals from the counter, each containing the voltage analog of the frequency of an individual burst, were averaged over 10 seconds with a VKI analog averager. The resulting voltage was read on a Simpson digital voltmeter. Signal quality was monitored with a Tektronix (model 7633) oscilloscope.

2.2.5 Seeding

The seeding of the flow was produced by a VKI smoke generator. This was supplied with air at a pressure of 1.7 bar and produced smoke particles of approximately 1 μm diameter as determined by a PARCO size analyzer. For the present low speed, low acceleration flow, particles of this size will accurately follow the local flow streamlines. Smoke was continuously introduced in the tunnel settling chamber, producing a relatively uniform distribution in the test section.

3. FLOW FIELD MEASUREMENTS

3.1 Freestream uniformity

As explained in section 2.1, the tunnel bottom and top walls were slightly diverging (the angle of divergence was 2° from the tunnel axis for each wall) to account for the boundary layer growth along them. To check that the divergence was correct, the flow field in the tunnel was surveyed without any model installed. LDV velocity surveys were performed in the tunnel center plane from the bottom wall to the top wall. They were carried out at three different stations (at 31, 38 and 48 cm from the test section inlet) and at four different velocities (from 1 to 2.5 ms^{-1} by increment of 0.5 ms^{-1}). The results of the surveys are presented in figures 4-7. They indicate that the flow is effectively uniform in the test section, the better correction being at the lower end of the velocity range.

3.2 Two dimensionality of the flow

Velocity surveys were performed in the boundary layer over the elliptic cylinder at three transverse positions to check for transverse uniformity. These were at y = -5, 0, 5 mm from the tunnel center plane. Although this is not a sufficient condition of two dimensionality in general (Ref. 7), for this low speed flow at zero incidence, it is a strong indication of two dimensionality. A further indication is given by Abbott & Von Doenhoff (Ref. 8) in which two dimensional NACA aerofoil data are reported. These were obtained for an aspect ratio (span/chord) of 1.5. In this experiment, the aspect ratio is 3, i.e., a more favourable situation.

3.3 Effect of model configuration on resolution/quality of measurements

Boundary layer velocity profiles were collected in forward and backscatter modes for three tunnel/model configurations at V_∞ = 2 ms^{-1}. In configuration 1, the model was not painted and the tunnel walls were not covered. In configuration 2, the model was kept the same but the tunnel walls were covered with black paper to avoid stray light. Finally, in configuration 3, the model was painted matt black to minimize reflections.

Figure 9 shows a typical example of boundary layer profiles obtained in forward scatter for the three configurations. As expected, the same values of velocity were recorded in all measurement cases. It was observed that painting the model resulted in a marked reduction of reflections from the surface and in the associated improvement in the signal-to-noise ratio. The velocity profile shown in figure 9 was obtained at a station close to the ellipse leading edge where the boundary layer thickness is small (less than 1 mm). It exemplifies one of the problems in the measurements : determining the zero vertical location. Indeed, there obviously exists a zero-shift in the vertical scale of the figure (also in figure 8) since, at the wall, the velocity must be zero to satisfy the no-slip condition. Fortunately, laminar velocity profiles display a large nearly linear region and it is therefore easy to find the wall position by extrapolation of the velocity profiles. Once this has been done at one point, the coordinates of any point in the field can be known within the accuracy of the traversing mechanism. When this is done with the data of figure 9, it can be concluded that the first measurement point was taken at 0.08 mm from the wall.

3.4 Effect of scatter mode on resolution/quality of measurements

In figure 10, velocity profiles obtained in backscatter and forward scatter modes are compared for one of the configurations described in 3.3. It can be observed that velocity measurement could be obtained as close to the wall in backscatter as in forward scatter mode. However, in backscatter mode, the signal intensity is much smaller, resulting in a deteriorated signal-to-noise ratio. This does not represent a major problem for the present low speed flow but might be a serious difficulty in high speed flow.

3.5 Measurements in reverse flow regions

All previous measurements reported (sections 3.1-3.4) used a stationary fringe system which cannot resolve directional ambiguity. Also, due to the low measured speed and the relatively large interfringe distance, the frequencies processed were at the lower end of the range covered by the band-pass filters, resulting in a poor signal quality at low speed (poor filtering).

Therefore, Bragg cells were added to the LDV setup (Fig. 3). In addition, as mentioned in section 2.2.2, the 15 mW red laser source was replaced with a 4 watt green laser because the photomultiplier has a better quantum efficiency for green light than for red light. Finally, the focal length of the lens which causes the beams to cross was reduced to 110 mm to improve the resolution. These changes appear in Table 1.

With the LDV parameters indicated in Table 1, the doppler shift corresponding to 2 ms^{-1} was 0.78 MHz. A Bragg cell frequency of 1.3 MHz, i.e., more than 1.5 times the value for the incoming stream was selected. This produced signals having frequencies more amenable to effective filtering.

Measurements were performed at a freestream velocity of 2 ms^{-1} at four stations from the ellipse mid chord to a station in the wake. The velocity profiles are shown in figures 11-14. First, measurements could be performed within 0.05 mm from the wall with Bragg cells. Secondly, the velocity profiles exhibit negative velocities at all stations, even at the ellipse mid chord. This may appear surprising as one would expect separation downstream of the mid chord but a similar behaviour was observed by Schubauer (Refs. 9-10) with an elliptic cylinder of ratio (2.95:1). Negative velocities are also recorded in the wake at 15 mm (i.e., 37 percent of the chord) downstream of the trailing edge. This indicates the presence of a very elongated separation bubble downstream of the elliptic cylinder. Finally, the wake velocity profile shows that the flow is symmetrical under the test conditions used.

4. COMPARISON WITH A BOUNDARY LAYER COMPUTATION

The laminar boundary layer around the elliptic cylinder was calculated with the computer code developed by Arina et al. (Ref. 11) using the potential distribution as the external boundary condition. This code deals with compressible boundary layers but has been proved to work well even at very low Mach numbers.

The calculation predicts separation at S/L' = 0.823 (L' = ellipse half perimeter), which is in agreement with the value computed by Schlichting (Ref. 12) using the method of Polhausen. This is much larger than observed experimentally since at mid chord (S/L' = 0.5), a reverse flow profile was recorded. The discrepancy is due to the viscous-inviscid interaction at separation which is not accounted for by the theory. A similar and well known phenomenon exists for the circular cylinder case (Ref. 12).

The comparison was therefore restricted to attached flow cases, i.e., stations upstream of the ellipse mid chord, as appears in figure 15. The agreement is good except near the leading edge. In this region, as discussed by Peyret-Viviand (Ref. 13), the viscous/inviscid coupling is strong at this intermediate Reynolds number (1350). To account for this coupling, and to predict accurately separation and separated flow profiles, a full Navier-Stokes calculation should be performed.

5. CONCLUSIONS

An experimental investigation of the low speed flow around an elliptic cylinder was performed. The problem addressed was the feasibility of performing LDV velocity measurements with a sufficient resolution close to a solid surface in a two dimensional separated flow with thin laminar boundary layers.

It was shown that velocity measurements could be obtained with very small probe volumes to within 0.05 mm from the surface both in attached and reverse flow regions, thus enabling an accurate description of the velocity profiles.

Painting the model with matt black paint and covering the tunnel walls proved to be effective means of improving signal quality. Measurements were successful both in back and forward scatter modes.

The velocity profiles measured with Bragg cells indicate that the flow is separated at the ellipse mid chord and that the separation bubble extends far downstream in the wake.

The velocity profiles in the attached flow region compare well with the results of a boundary layer computation.

REFERENCES

1. HAKKINEN, R.J. et al. The interaction of an oblique shock wave with a laminar boundary layer.
NASA Memo 2-18-59W, March 1959.

2. BAROTH, E.C. & HOLT, M.: Investigation of supersonic separated flows in a compression corner by laser doppler anemometry.
Experiments in Fluids, Vol. 1, No. 4, 1983, pp 195-203.

3. GINOUX, J.J. & DEGREZ, G.: Three dimensional skewed shock wave laminar boundary layer interaction : laminar and turbulent behaviour.
AFOSR Final Scientific Report, Grant AFOSR 82-0051, December 1982; also VKI CR 1983-05/AR.

4. DEGREZ, G. & GINOUX, J.J.: Three dimensional skewed shock wave laminar boundary layer interaction at Mach 2.25.
AIAA Paper 83-1755, to be published in AIAA Journal; also VKI Preprint 1983-04.

5. PANKHURST, R.C. & HOLDER, D.W.: Wind tunnel technique.
London, Pitman & Sons, 1952.

6. DURST, F.; MELLING, A.; WHITELAW, J.H.: Principles and practice of laser-doppler anelometry.
London, Academic Press, 1970.

7. HANKEY, W.L. & HOLDEN, M.S.: Two dimensional shock wave boundary layer interactions in high speed flows.
AGARDograph No. 203, June 1975.

8. ABBOTT, I.H. & VON DOENHOFF, A.E.: Theory of wing sections.
New York, Dover, 1959.

9. SCHUBAUER, G.B.: Air flow in separating boundary layer.
NACA TR 527, 1935.

10. SCHUBAUER, G.B.: Air flow in the boundary layer of an elliptic cylinder.
NACA TR 652, 1939.

11. ARINA, R. & ESSERS, J.A.: A finite difference technique for laminar and turbulent compressible boundary layers. In "Introduction to Computational Fluid Dynamics",
VKI LS 1983-01, January 24-28 1983.

12. SCHLICHTING, H.: Boundary layer theory.
New York, McGraw-Hill, 1979.

13.. PEYRET, R. & VIVIAND, H.: Computation of viscous compressible flows based on the Navier-Stokes equations.
AGARDograph 212, 1975.

		Sections 3.1-3.4	Section 3.5
Beam separation, d	λ	0.6329 μm	0.5145 μm
Focal length, f	d	35 mm	22.4 mm
Beam diameter, D_{e-2}	D_{e-2}	2.49 mm	3.40 mm
Laser wavelength, λ	f	200 mm	110 mm
Angle of intersection, 2ϕ $\quad \phi = \arctan(d/2f)$	ϕ	5.0°	5.8°
Interfringe distance, d_f $\quad d_f = \lambda/2\sin\phi$	d_f	3.63 μm	2.54 μm
Beam waist, d_{e-2} $\quad d_{e-2} = 4\lambda f/\pi D_{e-2}$	d_{e-2}	64.7 μm	21.2 μm
Width of probe volume, d_m $\quad d_m = d_{e-2}/\cos\phi$	d_m	65.0 μm	21.3 μm
Length of probe volume, ℓ_m $\quad \ell_m = d_{e-2}/\sin\phi$	ℓ_m	0.743 mm	0.209 mm
Number of fringes, N_{fr} $\quad N_{fr} = d_m/d_f \cong \frac{4d}{\pi D_{e-2}}$	N_{fr}	17.9	8.4

TABLE 1 - LASER DOPPLER VELOCIMETRY PARAMETERS AND EQUATIONS

1. LOW SPEED FLOW OVER AN ELLIPTIC CYLINDER

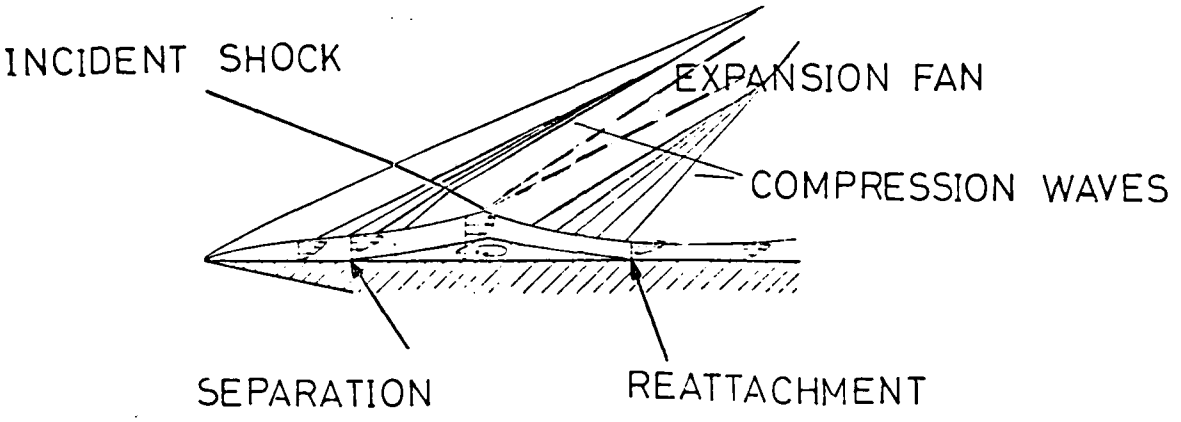

2. INCIDENT SHOCK BOUNDARY LAYER INTERACTION

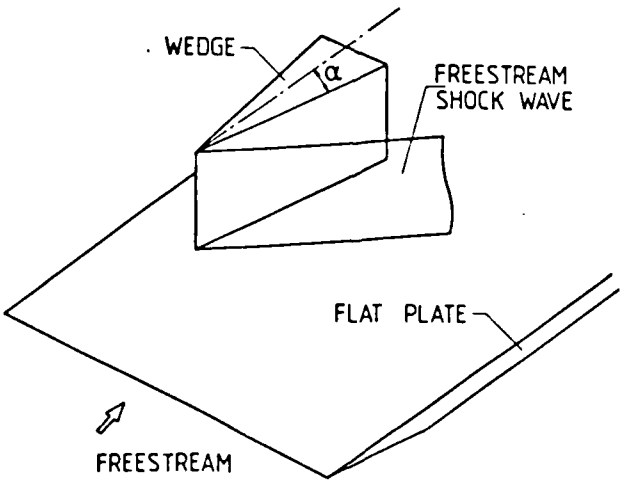

3. 3D SKEWED SHOCK BOUNDARY LAYER INTERACTION

FIG. 1 - ORGANIZATION OF EXPERIMENTAL PROGRAM

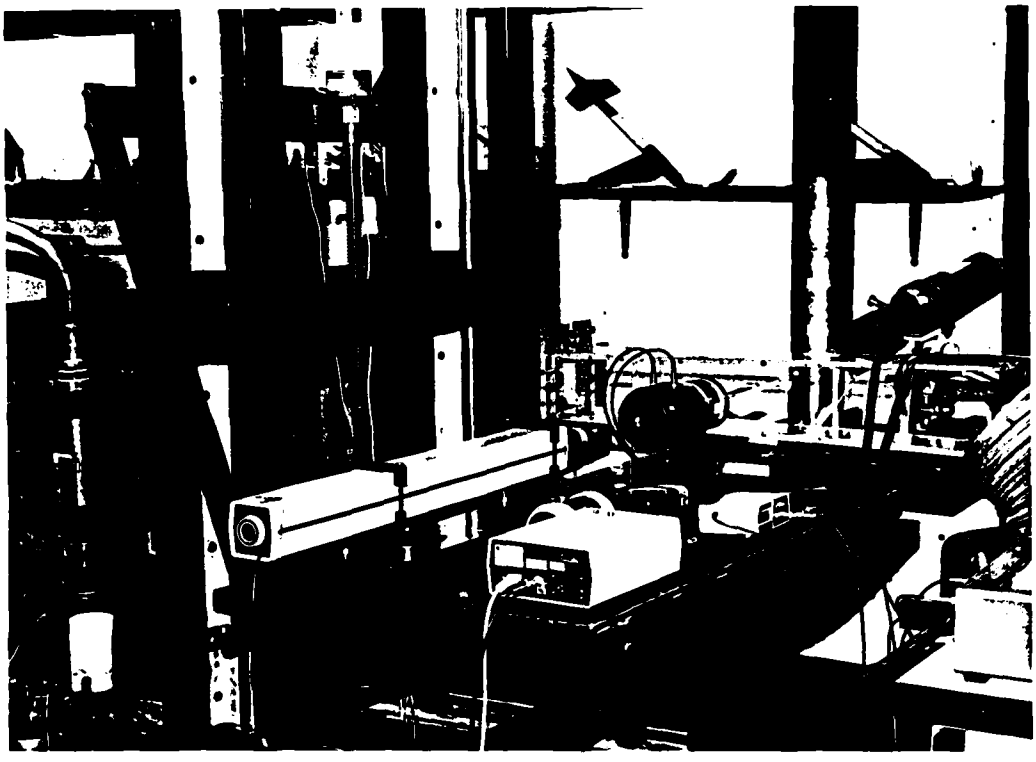

FIG. 2 - EXPERIMENTAL SETUP

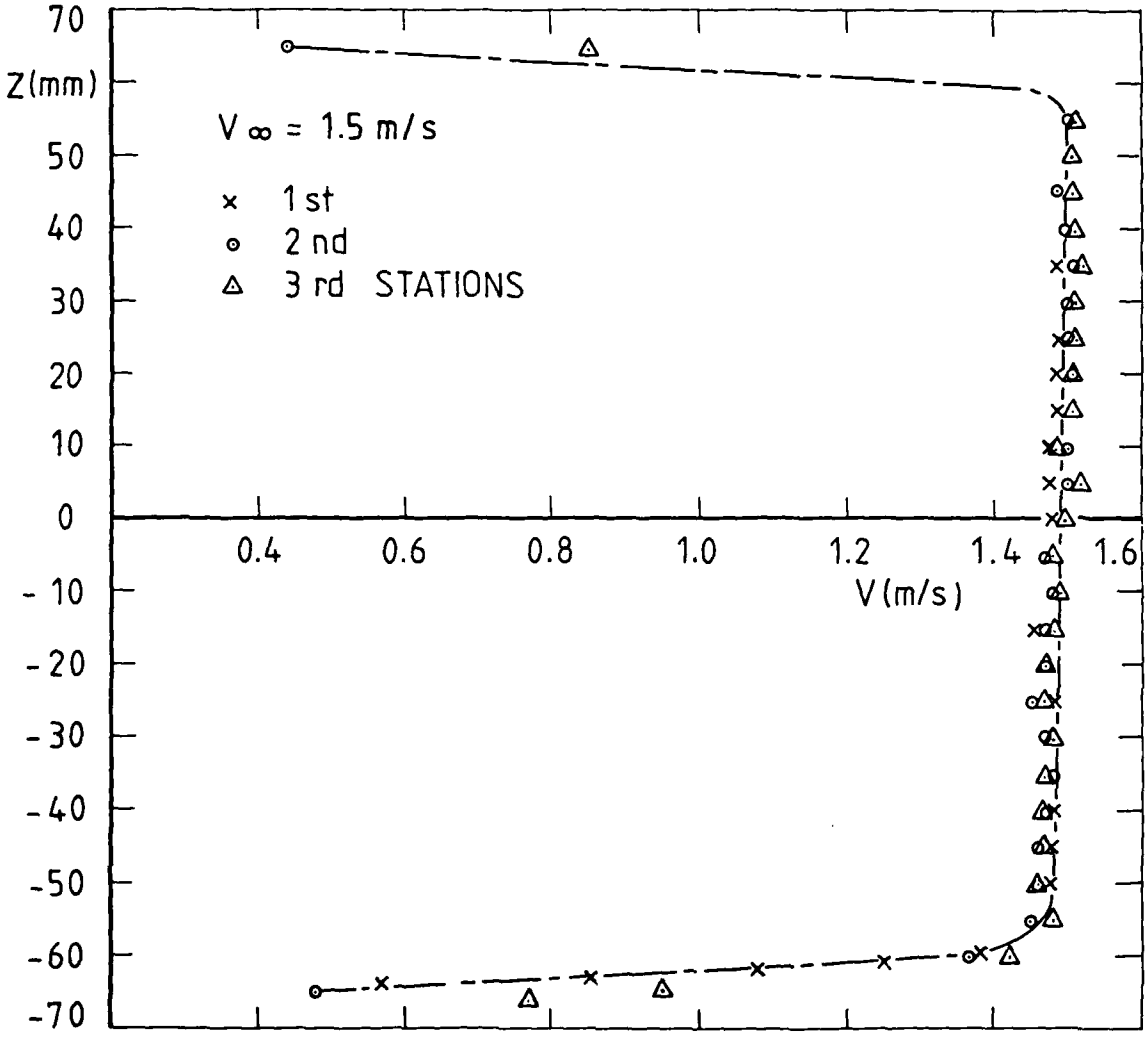

FIG. 5 - FREESTREAM SURVEYS AT u_∞ = 1.5 ms^{-1}

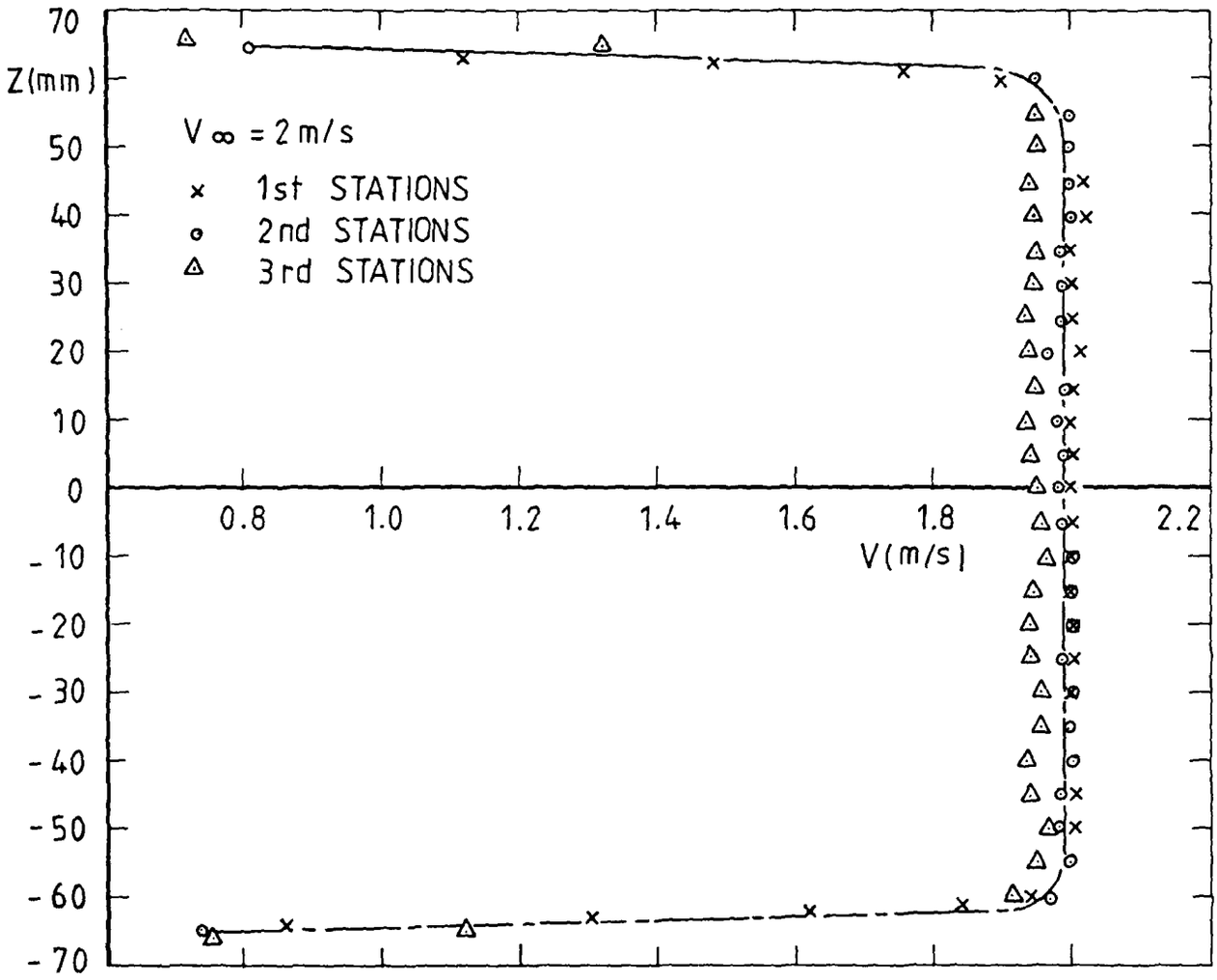

FIG. 6 - FREESTREAM SURVEYS AT $u_\infty = 2\ ms^{-1}$

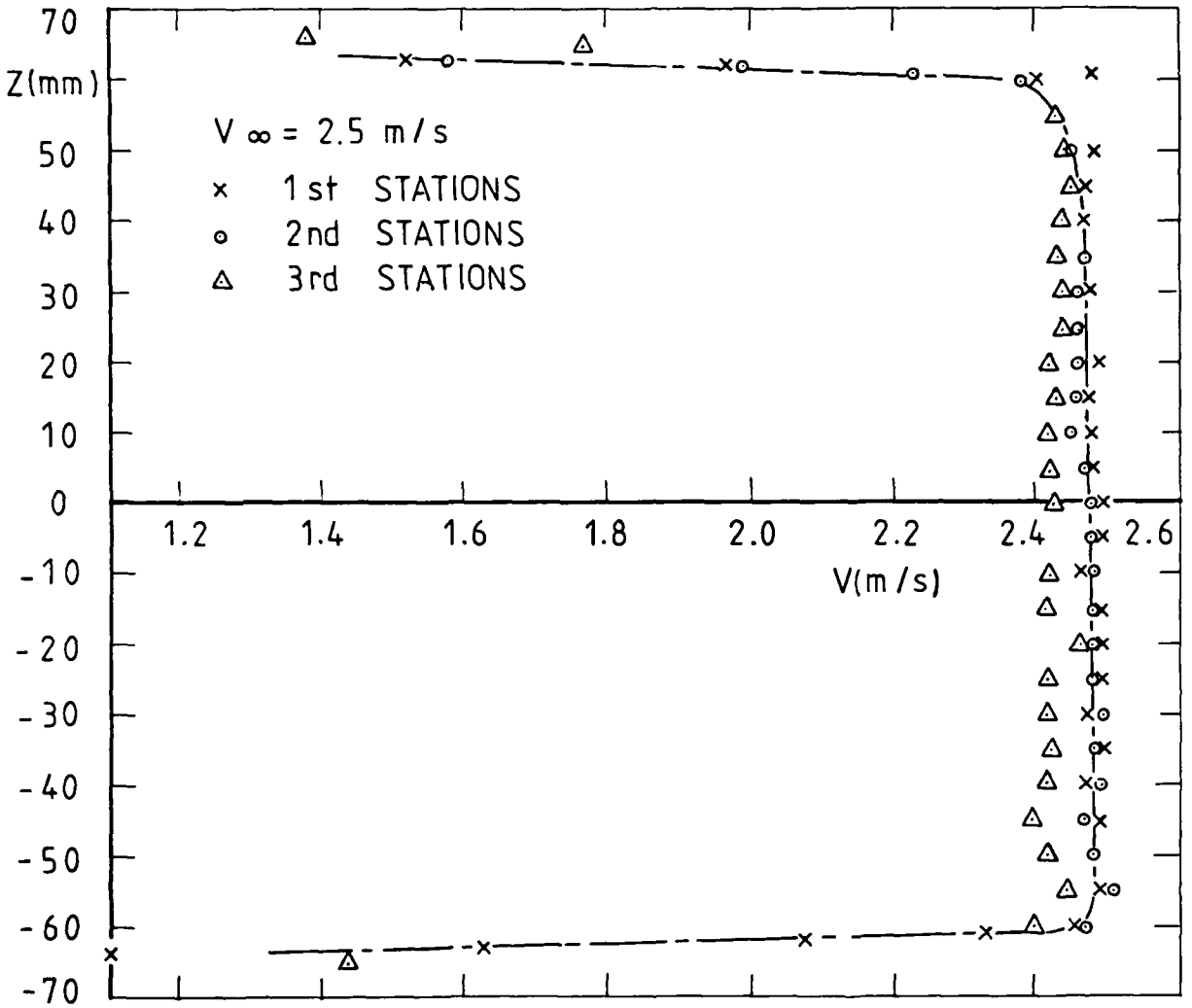

FIG. 7 - FREESTREAM SURVEYS AT u_∞ = 2.5 ms^{-1}

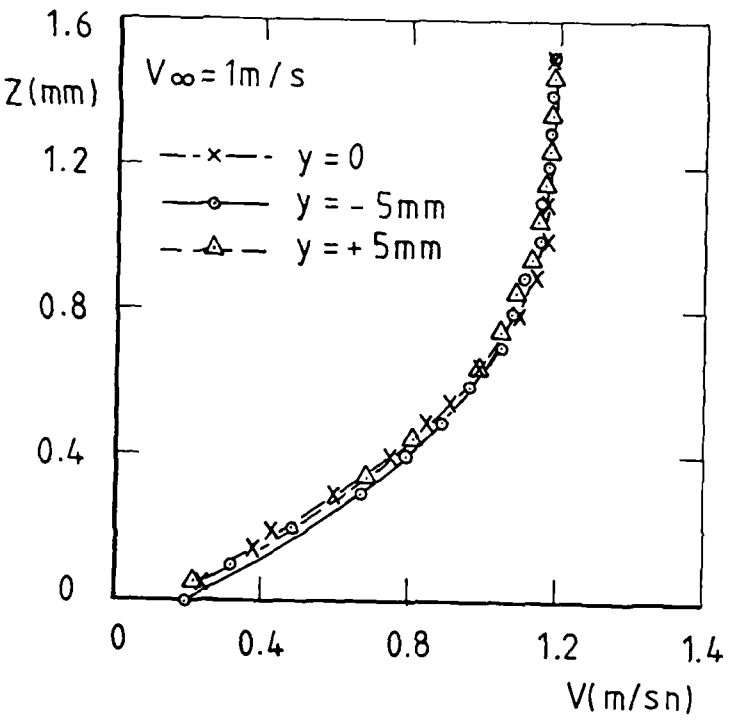

FIG. 8 - BOUNDARY LAYER PROFILES - TRANSVERSE UNIFORMITY

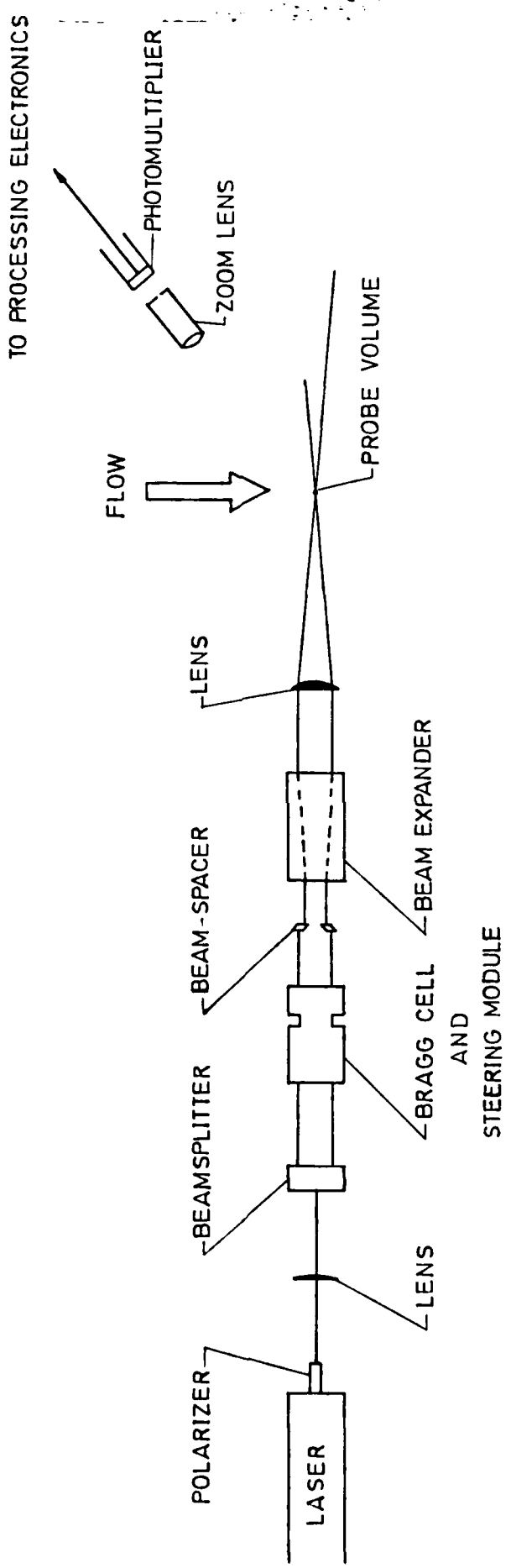

FIG. 3 - SCHEMATIC OF LDV SYSTEM

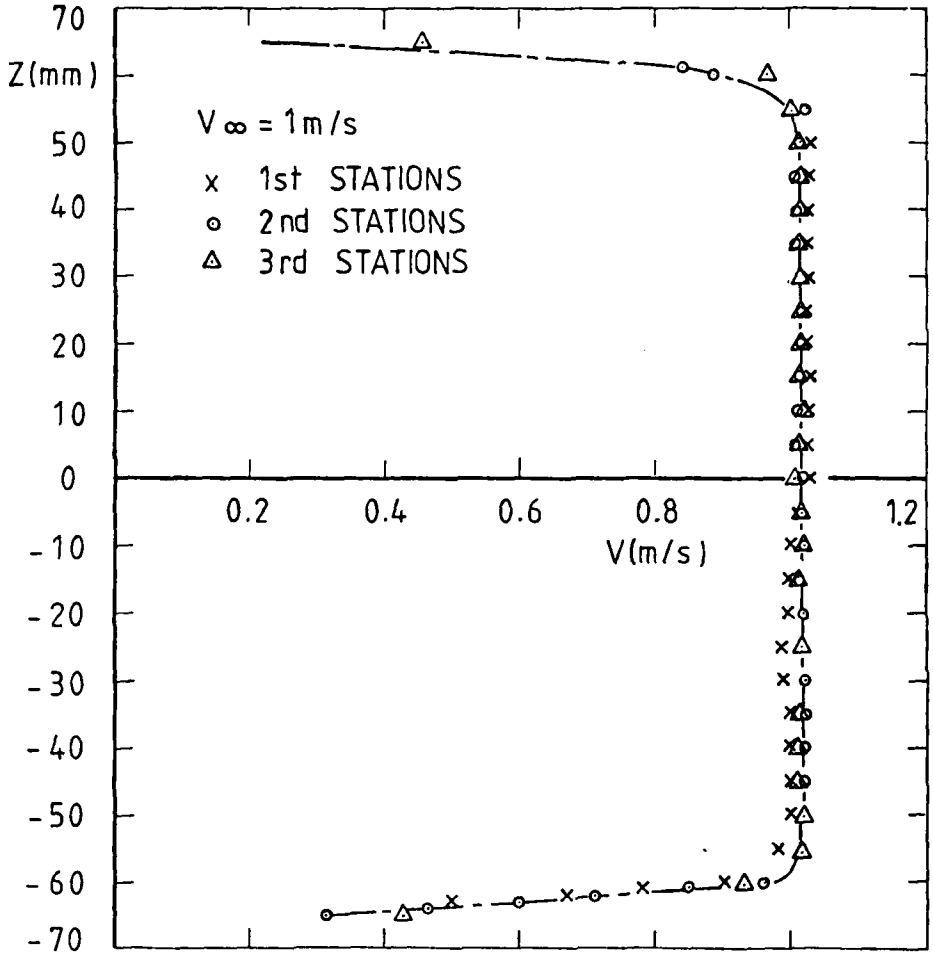

FIG. 4 - FREESTREAM SURVEYS AT $u_\infty = 1\ ms^{-1}$

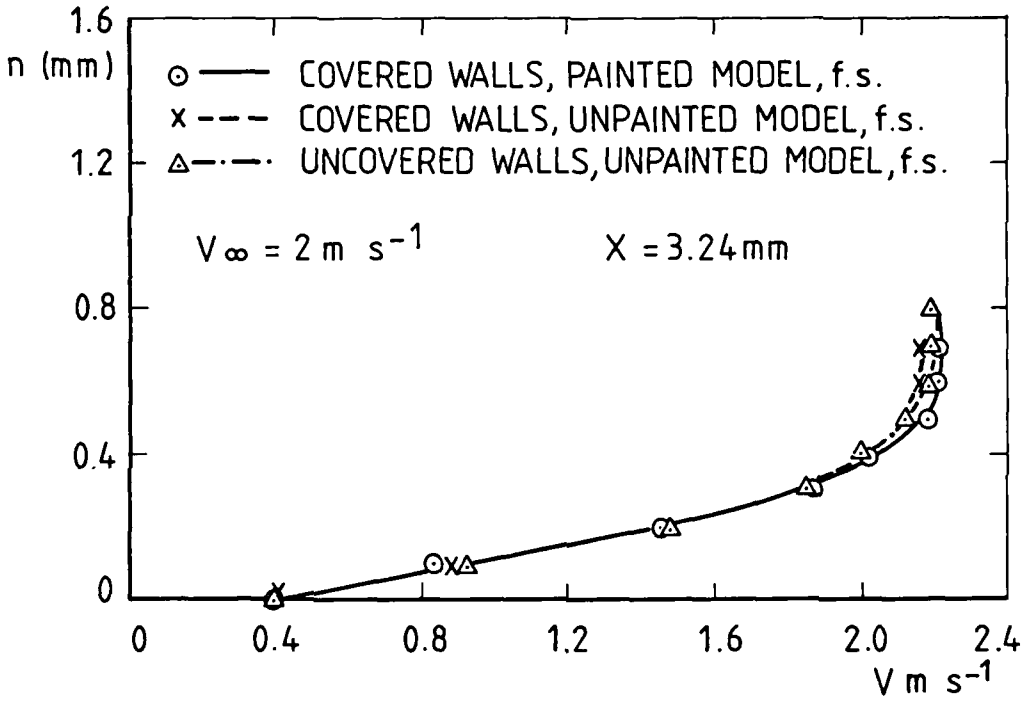

FIG. 9 - BOUNDARY LAYER PROFILES - EFFECT OF MODEL CONFIGURATION

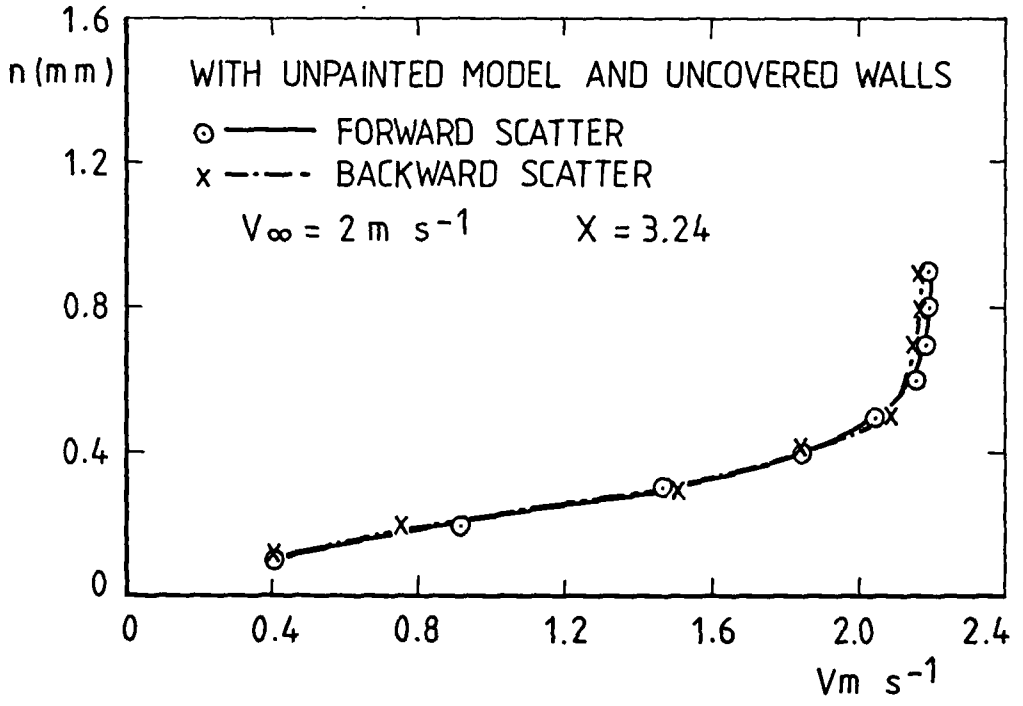

FIG. 10 - BOUNDARY LAYER PROFILES - EFFECT OF SCATTERING MODE

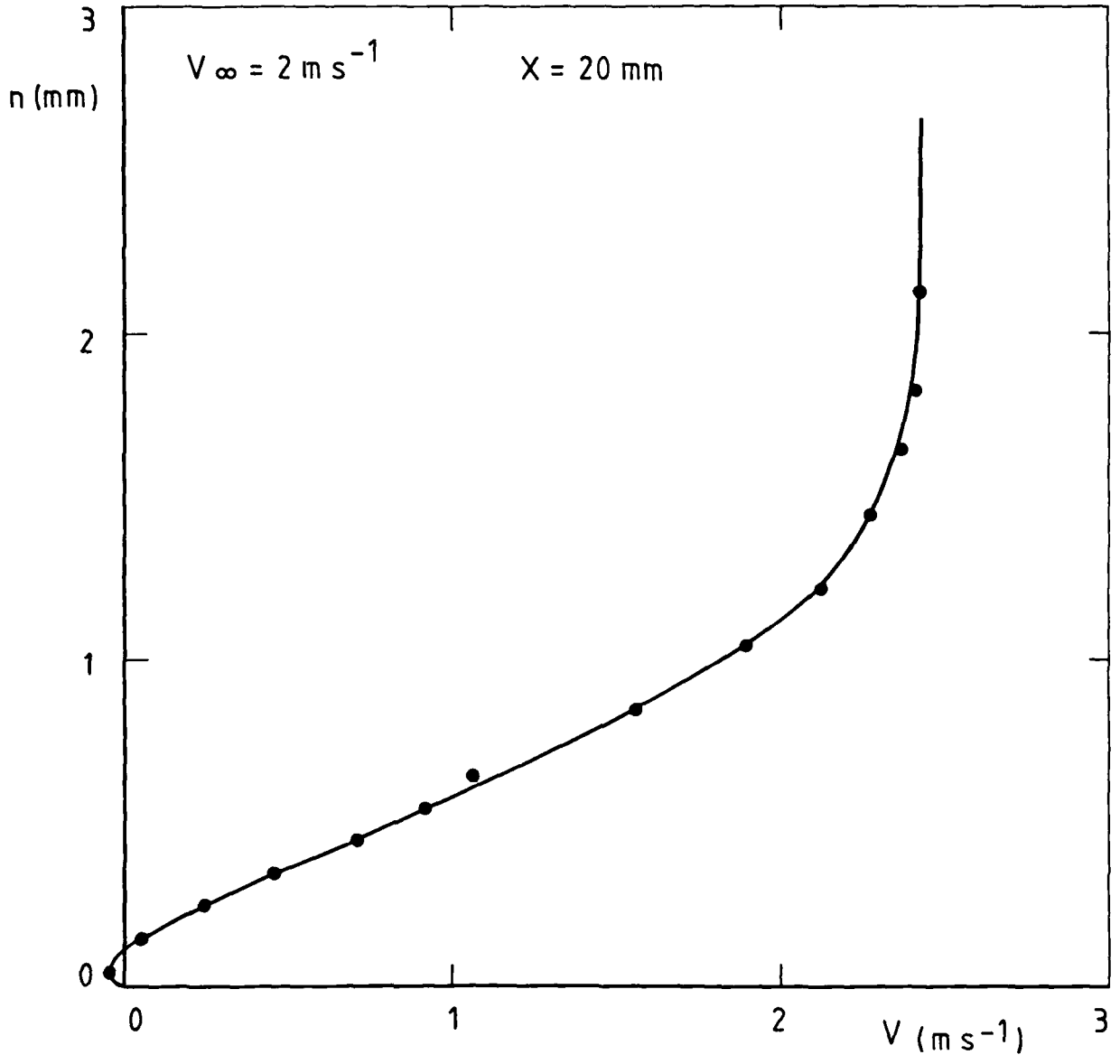

FIG. 11 - BOUNDARY LAYER PROFILES WITH BRAGG CELLS x = 20 mm

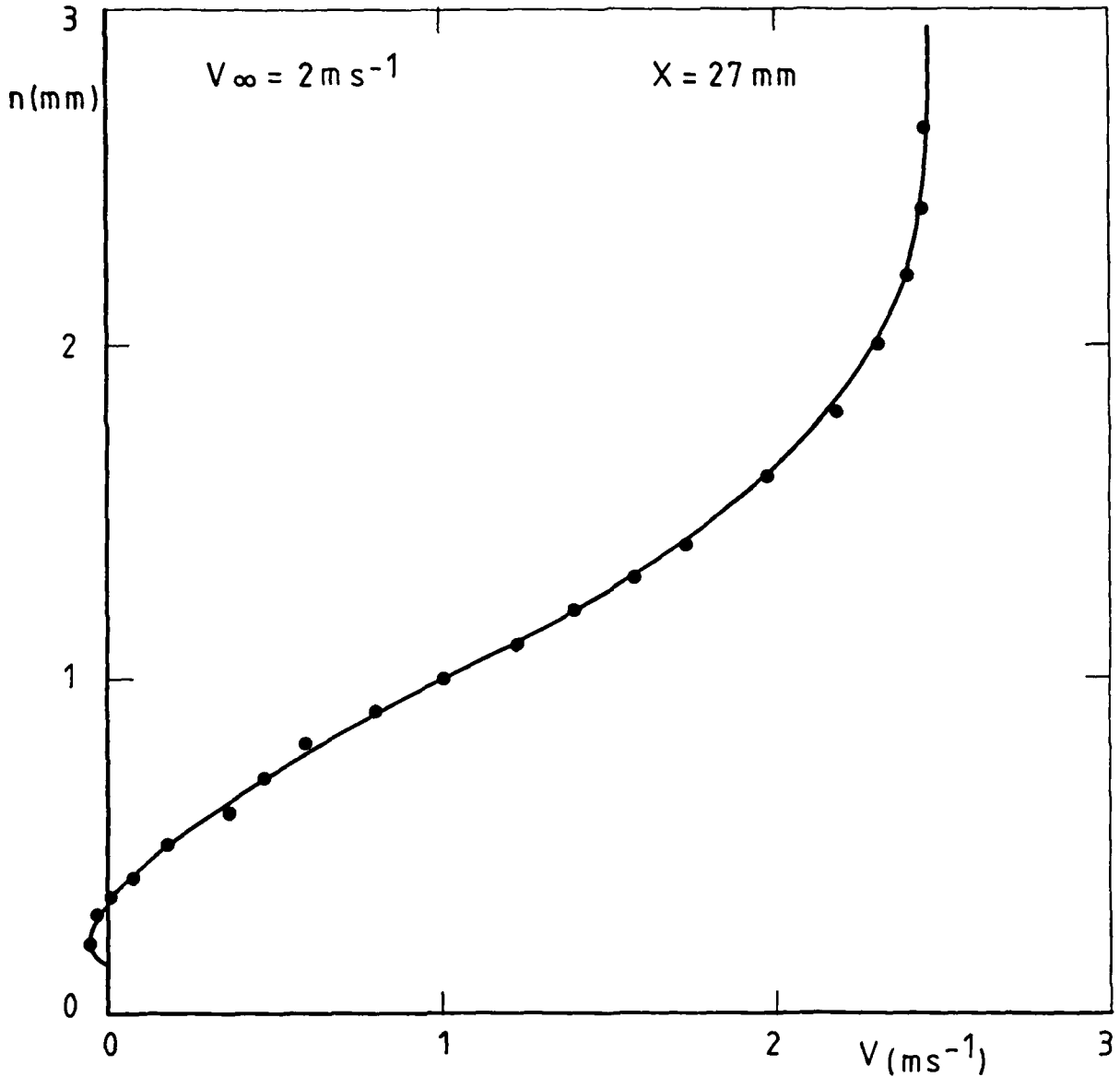

FIG. 12 - BOUNDARY LAYER PROFILES WITH BRAGG CELLS x = 27 mm

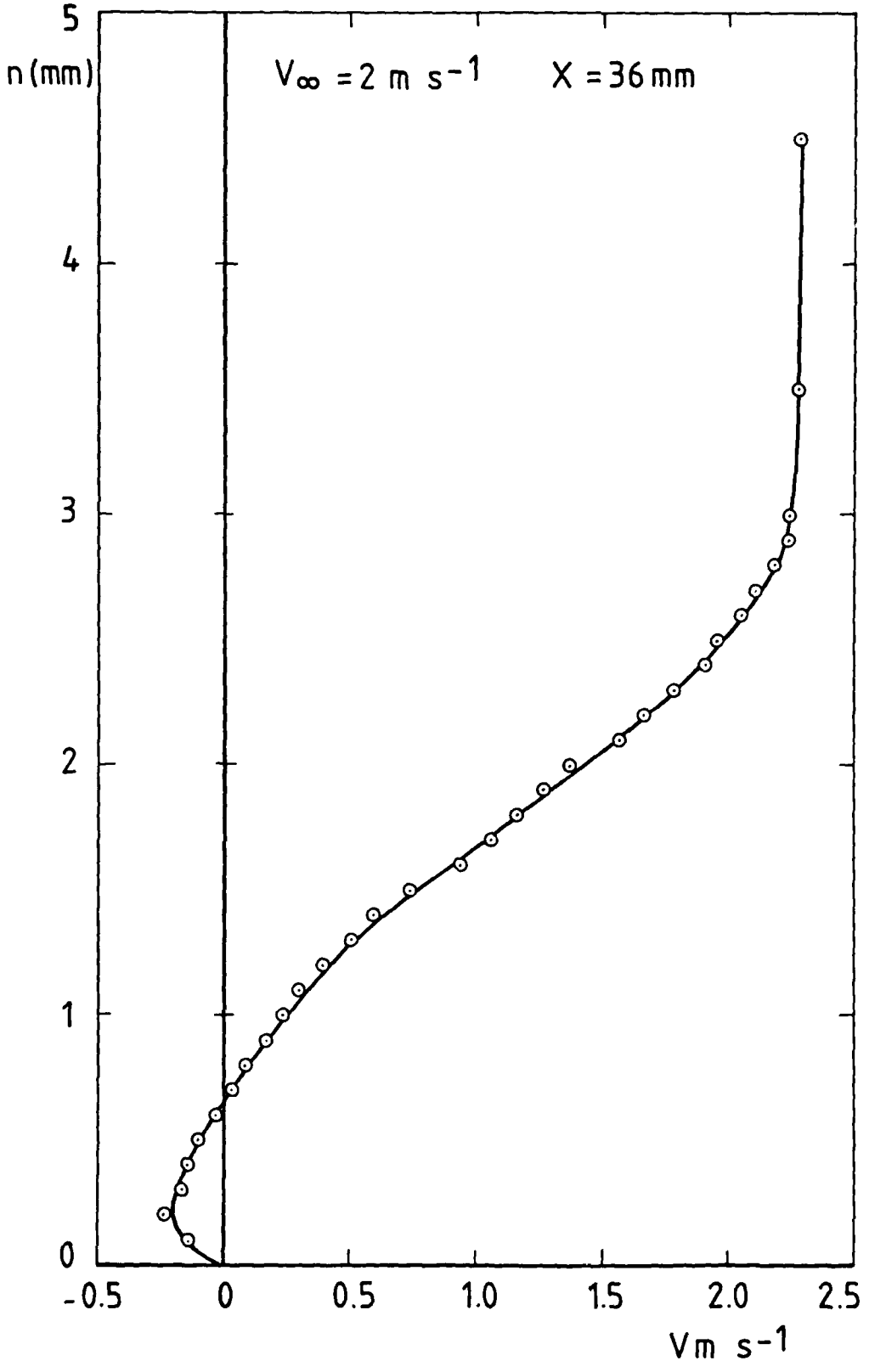

FIG. 13 - BOUNDARY LAYER PROFILES WITH BRAGG CELLS x = 36 mm

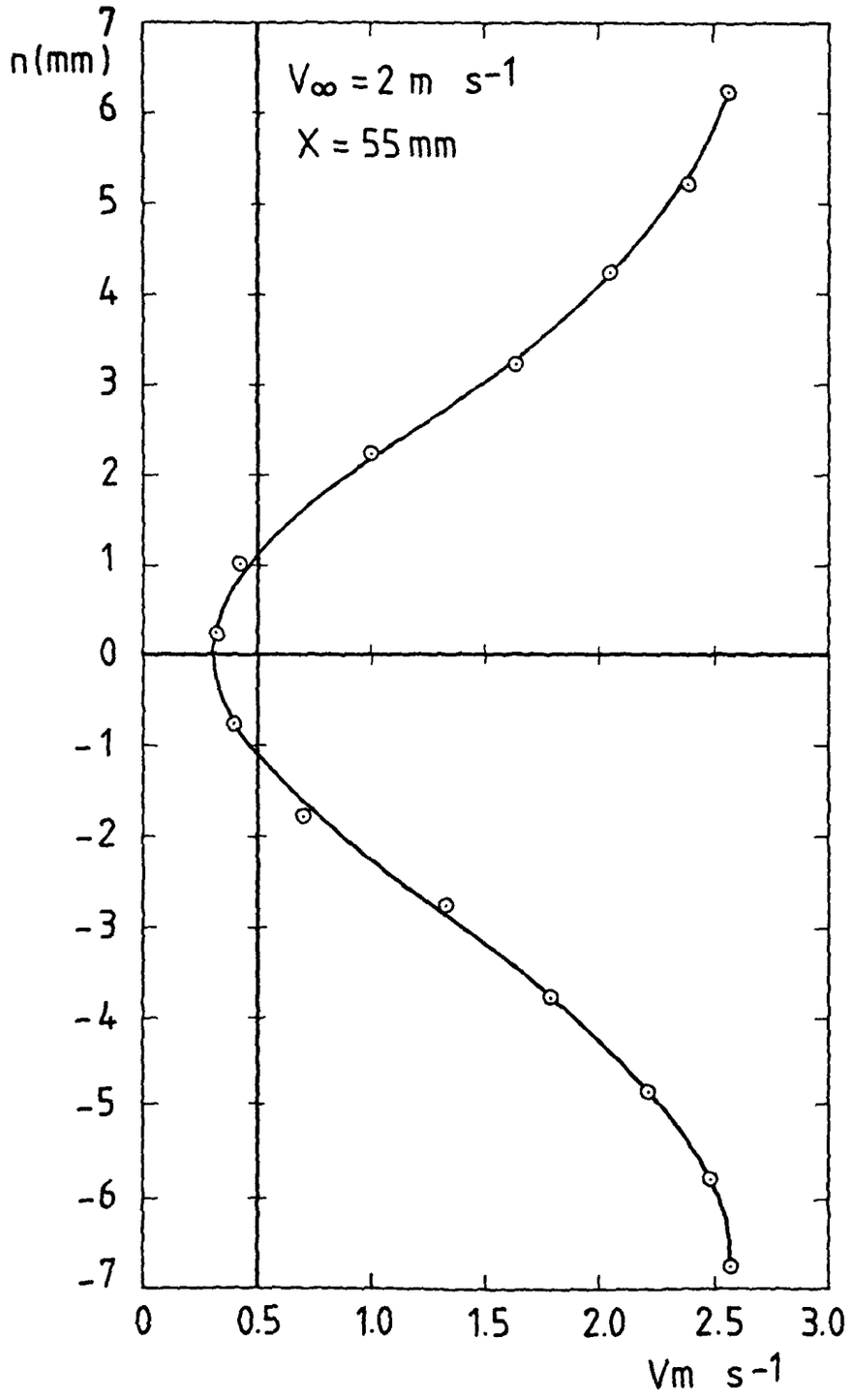

FIG. 14 - BOUNDARY LAYER PROFILES WITH BRAGG CELLS x = 55 mm

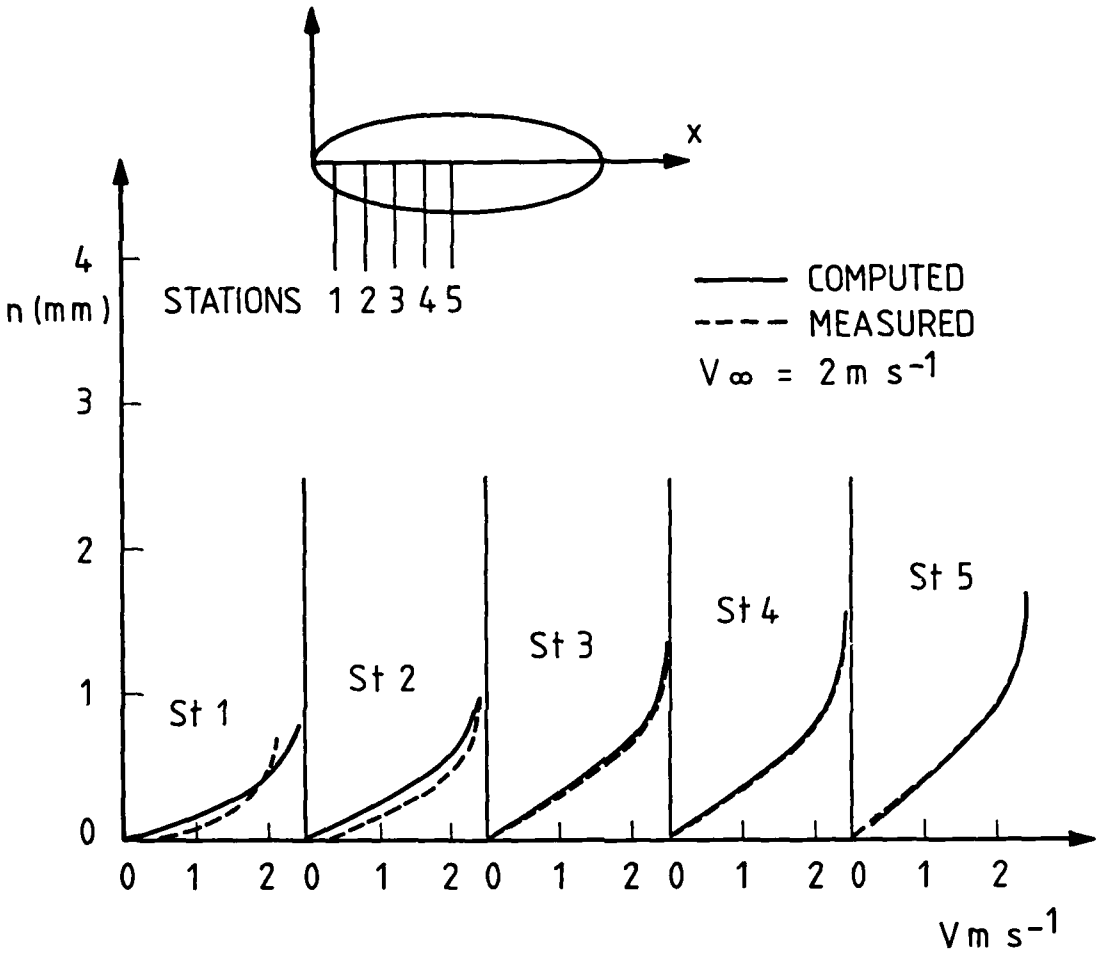

FIG. 15 - COMPARISON OF MEASURED VELOCITY PROFILES AND BOUNDARY LAYER

END

FILMED

2-85

DTIC